Quantum Electronics **51** (6) 554–561 (2021)

LASER GYROSCOPES https://doi.org/10.1070/QEL17541

Multimode semiconductor laser gyroscope and factors determining its operation

V.K. Sakharov

Abstract. **We report the results of a study of a multimode semiconductor laser gyroscope (MSLG) with a long fibre-optic ring cavity (RC) and alternating frequency dithering formed by a lithium niobate phase modulator, and discuss the factors that determine the device operation. The fundamental limitations in MSLG operation are phase fluctuations and the multimode nature of radiation. Phase fluctuations caused by spontaneous emission of photons in a semiconductor optical amplifier (SOA) result in a slow drop in the beat amplitude. However, its complete decay does not occur due to the periodic and short-term lock-in phenomenon, which leads to the equalisation of the fluctuation levels in pairs of counterpropagating waves (PCPWs) that form the RC modes, and, thereby, to the restoration of the beat amplitude. The limitations associated with the multimode lasing regime are overcome due to the fact that the emission spectrum consists of a small number of narrow lines, and the positions of the antinodes and nodes of standing waves in the SOA field distribution coincide or are close. Both factors lead to the mode locking in spectral lines and, as a consequence, to synchronisation of PCPW beats at the device output. The mechanism of the formation of these factors is not yet clear.**

Keywords: *laser gyroscope, lock-in, frequency dithering, phase fluctuations, wave beats, mode locking.*

1. Introduction

The problem of developing a semiconductor (solid-state) laser gyroscope as an alternative to the He–Ne gyroscope remains relevant. This work presents the results of a study of a multimode semiconductor laser gyroscope (MSLG) and discusses the factors that determine its operability.

The main problems in the development of this device are lock-in and multimode lasing. Lock-in is associated with backscattering of optical radiation, the level of which in a semiconductor optical amplifier (SOA) is very high and, accordingly, the so-called locking zone is large, while the multimode regime is due to a small intermode spacing in the emission spectrum of a laser with a cavity, even of a relatively short length. Therefore, beats only occurre at a high rotation speed, and their amplitude turns out to be so small that the useful signal can only be isolated from the noise with the help of a radio frequency spectrometer, and the maximum sensitivity did not exceed 1 deg s^{-1} [1–4].

However, from the lock-in model proposed in work [5], it follows that the locking zone can be reduced using a ring cavity (RC) in the form of an extended fibre, and this allows the use of a alternating frequency dithering (AFD), which is quite simply formed by intracavity phase modulation. As shown in work [5], the problem associated with the multimode nature of radiation could be solved by introducing single-mode radiation from an external laser into the RC.

This approach was planned to be implemented in an experiment, in which an optical fibre with a length of at least 500 m, together with a fibre piezoceramic phase modulator, would have to be used to form the AFD. However, the very first experiments have shown that even without the introduction of single-mode radiation, beats appear at the MSLG output when using the AFD, which are easily recorded by means of a conventional oscilloscope.

This unexpected and unexplained, but consistently repeated effect became the object of our further research. It was found that the device responded to rotation by increasing the beat frequency in one half-period of the frequency dithering and reducing it in the other. In this case, the beat amplitude in both AFD half-periods gradually decreased, but in short time intervals between the half-periods it was restored. The device sensitivity was 10–20 deg h^{-1} [6].

Subsequent work was dedicated to experimental and theoretical studies of various modifications of the MSLG optical scheme, variants of phase modulation and AFD, emission characteristics, and beat processing technique for zero drift compensation, as well as to the search for an explanation of the large beat amplitude under multimode lasing conditions. Some of the results have been published in works [7, 8], and other results are presented in this paper.

The first part of the paper, containing experimental results, describes a device that differs from the one considered in [6] by greater stability of the output signal and flexibility in the choice of AFD options due to the use of a polarisation-maintaining fibre and an electro-optical phase modulator (EOPM). An experiment using the EOPM is discussed, which allowed us to establish that lock-in provides a fast and periodic restoration of the beat amplitude.

The rest and most of the paper is dedicated to the theoretical study of phase fluctuations and the search for an explanation of the significant beat amplitude in the output signal. All calculations are of statistical nature and relate to the stationary regime of MSLG operation.

V.K. Sakharov JSC Center VOSPI, ul. Vvedenskogo 3, 117342 Moscow, Russia; e-mail: vk_sach@mail.ru

Received 17 February 2021; revision received 6 April 2021
Kvantovaya Elektronika **51** (6) 554–561 (2021)
Translated by M.A. Monastyrskiy

The role of the large RC length, which makes it possible to significantly reduce the level of phase fluctuations and the spectral width of modes, is discussed. The processes of accumulation and reduction of the difference of phase fluctuations in pairs of counter-propagating waves (PCPWs) that periodically replace each other are considered. These processes, which occur, respectively, both in half-periods of the AFD (as a result of spontaneous emission of photons), and in short time intervals between them (due to the lock-in effect), determine the dynamics of the beat amplitude in an individual PCPW.

The approach to explaining the significant beat amplitude is based on calculations that use the idea that the amplifying medium is a region where, by virtue of some mechanism, conditions are created that ensure the synchronicity of the beats for a PCPW set. The beats of an individual PCPW in the calculation are presented in the form of intensity oscillations with the same frequency, equal to the sum of the frequency dithering and the Sagnac signal frequency, and with phases that differ in a varying degree depending on the optical spectrum structure, the position of the device for radiation outcoupling from the RC, as well as the relative position of the antinodes of standing waves in the amplifying medium, which is one of the factors that ensure the synchronicity of the PCPW beats.

2. Optical scheme of the device and characteristics of emission

Figure 1 shows the MSLG block diagram, where an InGaAsP/InP structure based on five quantum wells with optical amplification near a wavelength of 1.55 μm is used as a SOA, a Panda fibre with a length of $L \approx 600$ m, wound into a coil, is used as an RC, and a lithium niobate phase modulator in a planar design is used as an EOPM.

The AFD is formed using intracavity phase modulation of counterpropagating waves, when periodic signals of various shapes (sinusoidal, triangular, sawtooth, etc.) with a modulation frequency of 0.7–2.5 kHz and an amplitude of up to 100 V are fed to the EOPM, forming beats at the output with a frequency of 20–50 kHz.

The counterpropagating waves are coupled out and combined by a 2×2 fibre coupler with a power ratio of 95/5 at the outputs. The coupler made of polarisation-maintaining fibres fused without polarisation control is built into the RC in such a way that it provides linear polarisation of the waves circulating in the cavity, while the polarisation of the output waves is random. In this case, the beat amplitude decreases to some extent, but this decrease is compensated for by the simplicity of coupler manufacture.

A dielectric mirror installed at the end-face of one of the coupler's output ports is used to combine the output waves and direct them to the photodetector. Part of the radiation of one of the low-power output waves, passing from one port of the coupler to the other, returns to the RC, but this does not complicate the AFD formation. The beats are recorded using a photodetector, at the output of which a low-pass filter with a cutoff band of 100 kHz is mounted to suppress intermode beats.

The beat amplitude in both AFD half-periods gradually decreases, but rapidly recovers in the intervals between half-periods. When the pump current increases from 80 μA (threshold level) to 200 μA, the oscillation dynamics remains unchanged and the beat amplitude increases, while at higher currents the beat amplitude decreases.

The optical spectrum is a structure of narrow lines against the background of a relatively wide low-intensity spectrum. The line spacing is 0.27–0.3 nm. At the threshold pump current and its slight excess, the number of lines is no more than 3–5; as the current increases to 200 mA (Fig. 2), the number of lines increases to 10–15, occupying the 3–4 nm band. At an even higher current, a second group of lines appears in the spectrum, shifted to longer wavelengths by 4–5 nm.

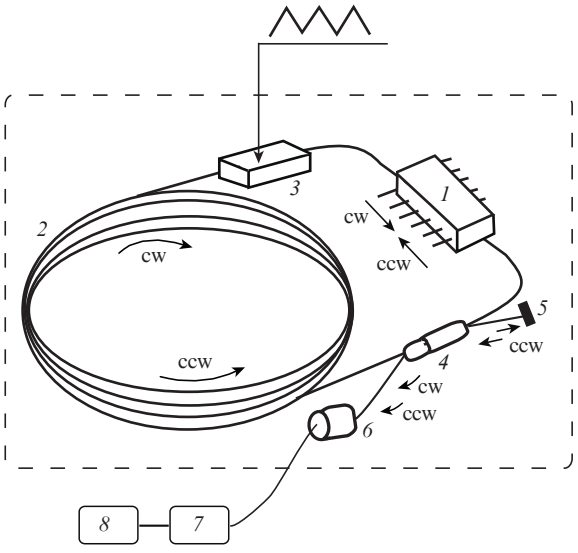

Figure 1. MSLG block diagram:
(*1*) SOA; (*2*) fibre coil; (*3*) EOPM; (*4*) fibre coupler; (*5*) mirror at the coupler's end face; (*6*) photodetector; (*7*) ADC; (*8*) personal computer.

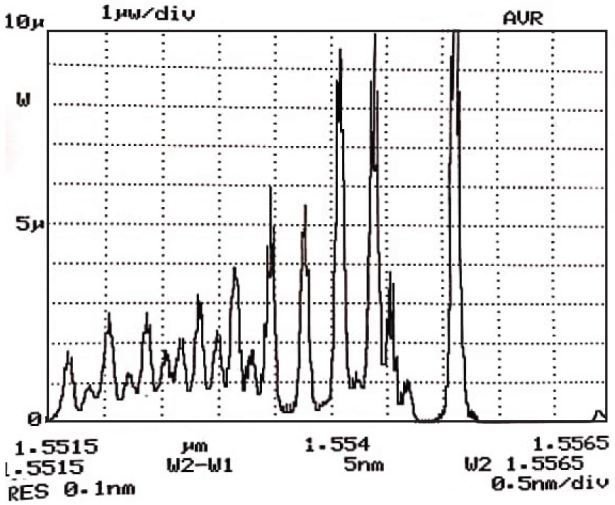

Figure 2. MSLG optical emission spectrum at a pump current of 150 mA.

The linewidth is not resolved by an optical spectrometer but can be estimated from the photocurrent spectrum. This spectrum, measured with a broadband photodetector and a radio spectrometer, is a frequency comb with a 335 kHz tooth interval equal to the intermode frequency; the frequency band occupied by the comb is 150–200 MHz, and the width of the teeth in the AFD absence is 1–2 kHz. This means that the average spectral linewidth is 1–1.5 pm, and the spectral width of the generated modes is about 1 kHz.

3. Constructive role of lock-in

The negative role of lock-in in the laser gyroscope operation is well known, which forms a zone of insensitivity to low rotation speeds and forces the use of a MSLG. However, it turns out that periodic and short-term lock-in between the AFD half-periods is of great importance for the MSLG operation.

This follows from the results of an experiment in which the application of the modulation signal $U(t)$ to the EOPM made it possible to easily change the phase modulation shape $F(t)$ and, accordingly, the frequency dithering $v_d(t)$ generated by it. We used modulation with signals in the form of a sinusoid and a triangle, the amplitudes of which remained unchanged, as well as modulation with a signal obtained by passing a triangular voltage through a double-diode limiter, while the modulation frequency v_m did not change, and the device itself was at rest.

In the case of intracavity phase modulation, frequency dithering $v_d(t)$ is determined by the expression [7]

$$v_d(t) = \frac{\Delta F(t)}{2\pi\tau}, \qquad (1)$$

where $\Delta F(t) = F(t-\tau^+) - F(t-\tau^-)$; $\tau^{\pm}$ is the travel time of waves from the phase modulator to the photodetector in the clockwise (+) and counterclockwise (–) directions; and τ is the travel time of waves along the entire RC length.

According to (1), for sinusoidal phase modulation $F(t) = F_0\sin(2\pi v_m t)$, the frequency dithering $v_d(t)$ is a harmonic function:

$$v_d(t) = \frac{\Delta\tau}{\tau} F_0 v_m \sin\left[2\pi v_m\left(t - \frac{\tau}{2}\right)\right], \qquad (2)$$

where F_0 is the phase modulation amplitude, and $\Delta\tau = |\tau^+ - \tau^-|$.

When modulated by a signal in the shape of an isosceles triangle, the frequency $v_d(t)$ has the shape of a meander:

$$v_d(t) = \frac{\Delta\tau}{\tau}\frac{2F_0}{\pi} v_m, \qquad (3)$$

and in the case of modulation by a triangle-shaped signal passed through a double-diode limiter, the $v_d(t)$ dependence differs from (3) by the appearance of small zones in which the frequency dithering is zero.

Figure 3 shows the modulation signals $U(t)$ and output beats $I(t)$ displayed on the monitor screen, and also frequency dithering $v_d(t)$ calculated using formulae (1)–(3). It can be seen that, in all three cases, the restoration of beat amplitudes occurs in the time intervals between the AFD half-periods, while the amplitude is lower in the case of modulation with a signal in the form of a triangle than in the other two cases. This means that the restoration of the beat amplitudes occurs due to lock-in, and the larger the amplitude, the longer the duration of its action. Thus, being a limiting factor in MSLG operation, lock-in simultaneously plays an important role, periodically restoring the beat amplitude.

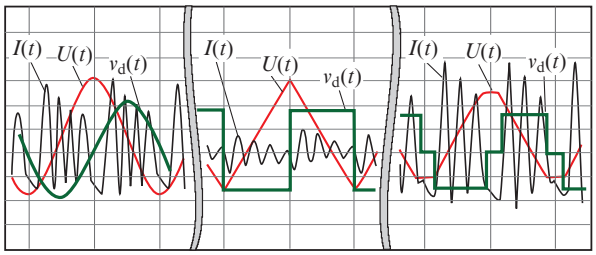

Figure 3. Signals of modulation $U(t)$ and beats $I(t)$ taken from the monitor screen and the calculated frequency dithering $v_d(t)$ for three variants of the SAFD at a modulation frequency of 2.23 kHz (see text).

4. Spontaneous emission, phase fluctuations, and spectral mode width

The source of the spectral broadening of laser modes is the spontaneous emission of photons in the amplifying medium. For a light wave with angular frequency ω and phase $\varphi(t)$, the normalised autocorrelation function of the radiation field can be represented as

$$G(t) = \langle\exp[i\tilde{\varphi}(t)]\rangle\exp(i\omega t), \qquad (4)$$

where $\tilde{\varphi}(t) = \varphi(t + t') - \varphi(t')$ are phase fluctuations (or random phases) and angle brackets indicate statistical averaging; it is assumed that amplitude fluctuations are smoothed out, and the radiation is considered single-mode.

For a single-mode laser diode (LD) with mirrors mounted at the crystal face ends, the phase fluctuations resulting from a large number of spontaneous emission events are considered as a normal, or Gaussian, process, which implies that

$$\langle\exp[i\tilde{\varphi}(t)]\rangle = \exp\left[-\frac{1}{2}\langle\tilde{\varphi}^2(t)\rangle\right], \qquad (5)$$

where the dispersion of phase fluctuations is

$$\langle\tilde{\varphi}^2(t)\rangle = \frac{R(1+\alpha^2)t}{2A}; \qquad (6)$$

R is the spontaneous emission rate; A is the average number of photons in the cavity; and α is the Henry factor [9]. The number of photons A is a measure of the ratio of the averaged intensities of the mode and radiation from a single act of spontaneous emission inside the amplifying medium.

According to the Wiener–Khinchin theorem and expressions (4)–(6), the spectral line shape in this case is Lorentzian with a full width at the 0.5 level from the maximum:

$$\Delta v = \frac{\langle \tilde{\varphi}^2(t) \rangle}{2\pi t}. \tag{7}$$

Consider a hypothetical external-cavity LD that generates a single mode. Suppose that its active element and optical losses are the same as in a single-mode LD with a radiation linewidth Δv, the external cavity is made in the form of a fibre with a length L, and the end faces of the crystal and the fibre have ideal antireflection coatings.

Since spontaneous photons affect the wave only when it passes through the amplifying medium, phase fluctuations in the radiation of this LD grow more slowly than in a single-mode LD, being distributed and averaged over the field of the entire extended cavity. Accordingly, the dispersion and width of the radiation spectrum decrease [10]:

$$\langle \tilde{\varphi}_L^2(t) \rangle \approx \langle \tilde{\varphi}^2(t) \rangle \frac{l_s n_s}{Ln}, \quad \Delta v_L \approx \Delta v \frac{l_s n_s}{Ln}, \tag{8}$$

where l_s is the semiconductor crystal length; and n and n_s are the refractive indices of the fibre and crystal.

Finally, let us turn to the MSLG, the active element and the optical losses of which are the same as in the considered single-mode external-cavity LD. It is natural to assume that the same mechanism of averaging phase fluctuations over the extended cavity field acts for each individual mode, so that the accumulation of phase fluctuations in the modes slows down. If we assume that for each mode, the ratio of its averaged intensity to the averaged intensity of radiation from an individual act of spontaneous emission, i.e., the number of photons, is the same as in the case of a single-mode LD, then the dispersion $\langle \tilde{\varphi}_{Lm}^2(t) \rangle$ and spectral width Δv_{Lm} of each mode will be determined by expressions similar to (8).

Thus, for an MSLG with parameters $L = 600$ m, $n = 1.47$, $l_s = 1.2$ mm, and $n_s = 3.6$, we obtain that the dispersion $\langle \tilde{\varphi}_{Lm}^2(t) \rangle$ and the mode width Δv_{Lm} are five orders of magnitude smaller than the corresponding parameters for a single-mode LD. Another important difference of the MSLG is that phase fluctuations in waves propagating in the RC in opposite directions are uncorrelated, although their dispersions $\langle \tilde{\varphi}_{Lm}^2(t) \rangle$ are the same.

5. Phase fluctuations and their dynamics when using AFD

The signal at the MSLG output is the sum of beats of a large number of PCPWs, each of them representing one of the modes involved in lasing. The beat amplitude of an individual PCPW corresponding to the ith mode is determined, as shown below, by the statistical distribution of the difference in phase fluctuations $\tilde{\xi}_i(t) = \tilde{\varphi}_i^+(t) - \tilde{\varphi}_i^-(t)$, where $\tilde{\varphi}_i^{\pm}(t)$ are the phase fluctuations in waves propagating in opposite directions. Assuming that the lasing conditions for all modes are the same, the phase fluctuations $\tilde{\varphi}_i^{\pm}(t)$ and their difference $\tilde{\xi}_i(t)$ are considered statistically identical and denoted hereinafter as $\tilde{\varphi}^{\pm}(t)$ and $\tilde{\xi}(t)$.

Obviously, the dynamics of the phase fluctuations $\tilde{\varphi}^{\pm}(t)$ and their difference $\tilde{\xi}(t)$, and, consequently, the dynamics of the beat amplitude of individual PCPWs, is different in periodically replacing time intervals, when the frequency dithering $v_d(t)$ is large enough to suppress lock-in, or when, on the contrary, it is small or even zero and therefore cannot suppress lock-in. The duration of the first intervals is denoted as τ_{dither}, and the duration of the second intervals as τ_{lock}; herewith $\tau_{dither} > \tau_{lock}$ and $\tau_{dither} + \tau_{lock} = T/2$, where T is the AFD period.

5.1. Dynamics of phase fluctuations in time intervals τ_{dither}

We divide the entire time interval τ_{dither} into N intervals of equal duration τ (travel time of waves along the entire RC length) and represent the difference of phase fluctuations $\tilde{\xi}(t_p)$ at time moments t_p ($t_p = p\tau$, $p = 1, \ldots, N$) as the sum of two terms:

$$\tilde{\xi}(t_p) = \tilde{\xi}(t_{p-1}) + \tilde{\eta}(\tau), \tag{9}$$

where $\tilde{\eta}(\tau)$ is the difference of phase fluctuations occurring at the current time interval.

Obviously, the difference $\tilde{\eta}(\tau)$ does not depend on the mode index and refers to stationary Gaussian processes with zero mean, and its dispersion $\sigma^2(\tau)$ is equal to the doubled dispersion of random phases of a multimode external-cavity LD, i.e., $\sigma^2(\tau) = 2\langle \tilde{\varphi}_{Lm}^2(t) \rangle$. Consequently, the distribution function of the difference $\tilde{\eta}(\tau)$ of random phases is

$$W_\eta(t_p, \phi) = \frac{1}{\sigma(\tau)\sqrt{2\pi}} \exp\left[-\frac{\phi^2}{2\sigma^2(\tau)} \right]. \tag{10}$$

The distribution $W_\eta(t_p, \phi)$ is normalised on the interval $(-\pi, \pi)$, and its physical meaning is that the product $W_\eta(\tau, \phi)\mathrm{d}\phi$ determines the probability of finding the difference $\tilde{\eta}(\tau)$ of random phases in the interval $(\phi, \phi + \mathrm{d}\phi)$.

The difference $\tilde{\xi}(t_p)$ of random phases is not a Gaussian process, and its distribution $W(t_p, \phi)$, according to the law of distribution of the sum of two independent random variables, is determined by the convolution equation

$$W(t_p, \phi) = W(t_{p-1}, \phi) \otimes W_\eta(t_p, \phi). \tag{11}$$

Figure 4 shows the dynamics of the distribution $W(t_p, \phi)$ in the stationary regime in the time intervals τ_{dither} and τ_{lock}. The calculation relied on the use of the previous values of the parameters L, n, l_s, and n_s with the mode width $\Delta v_{Lm} = 1$ kHz, phase modulation frequency $v_m = 0.9$ kHz, backscattering coefficient $\gamma = 35$ dB, and time intervals τ_{dither} and τ_{lock}, which, respectively, amounted to 87% and 13% of the phase modulation half-period. It is seen that over the entire time interval τ_{dither}, the distribution $W(t_p, \phi)$ calculated using expressions (6) and (7) gradually broadens, with the initial distribution in this interval being the distribution $W(t_0, \phi)$ with a small width and a sharp maximum, formed in the course of lock-in, i.e., in the time interval τ_{lock}. It is easy to show that the distribution $W(t_N, \phi)$ broadens the faster the larger the width Δv_{Lm} of the modes, and at the end of the interval τ_{lock} it becomes virtually Gaussian.

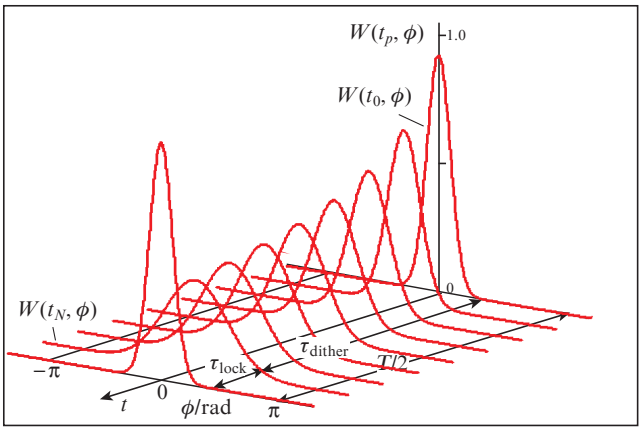

Figure 4. Dynamics of the distribution function $W(t_p, \phi)$ on the phase modulation half-period.

5.2. Dynamics of phase fluctuations in time intervals τ_{lock}

As was established above, the beat amplitude restoration occurs due to lock-in. To explain this effect, we use the model of a single-mode laser gyroscope [7], assuming that it is applicable for calculating the dynamics of the complex amplitudes of any PCW in the radiation of the device under consideration.

Then, in the absence of frequency dithering and rotation, using the recurrent equations (6) from work [7], the interaction of counterpropagating waves, the amplitudes of which are equal, and the phases are random, can be expressed as:

$$\exp[i\tilde{\varphi}^{\pm}(t_p)] = \exp[i\tilde{\varphi}^{\pm}(t_{p-1})] + \sqrt{\gamma}\exp[i\tilde{\varphi}^{\mp}(t_{p-1})], \qquad (12)$$

where p is the circulation number counted from the start of the frequency lock action; the second summands in the right-hand sides are the waves resulting from backscattering; and the polarisation of all waves, including the 'reverse' ones, is linear.

The dynamics of phase fluctuations $\tilde{\varphi}^{\pm}(t_p)$ in the time interval τ_{lock} represent, according to (12), the processes of equalisation of these fluctuations and, consequently, reducing the absolute value of their difference $\tilde{\xi}(t_p)$. The larger the backscattering coefficient γ and the time τ_{lock}, the higher the rate of decrease in the absolute value $\tilde{\xi}(t_p)$ and the smaller its final value. In this case, the calculated phase fluctuation difference $\tilde{\xi}(t_p)$ virtually does not depend on the choice of initial values $\tilde{\varphi}^{\pm}(t_0)$ corresponding to the same fixed initial value of the phase fluctuation difference $\tilde{\xi}(t_0)$.

To calculate the distribution obtained as a result of lock-in, an array of phases is used $\{\phi_k\}$, the elements of which are uniformly distributed in the interval $(-\pi, \pi)$, and an array of samples of the distribution $W(t_N, \phi)$, formed at the end of the time interval τ_{dither}, i.e., an array $\{w_k\}$, the elements of which are defined as $w_k = W(t_N, \phi_k)$; the number of elements in both arrays is quite large. For each pair of elements (ϕ_k, w_k), the phase shift $\Delta\phi_k$ that occurs during the process of lock-in is calculated using expressions (12). In this case, the initial values of the random phases, $\tilde{\varphi}^{\pm}(t_0) = \pm\phi_k/2$, the operation time τ_{lock} of lock-in, during which the counter-propagating waves make a small number of circulations, and other necessary parameters are set.

Since any distribution function is actually a histogram, the phase shifts $\{\Delta\phi_k\}$ cause the histogram bars corresponding to each initial pair of elements (ϕ_k, w_k) to move towards the centre; in some areas these bars overlap each other, while in other areas certain gaps appear between them. Taking into account the displacements and heights of a large number of bars of the distribution-histogram $W(t_N, \phi_k)$ allows us to calculate the desired distribution $W(t_0, \phi)$, which remains normalised, while its width decreases, and the resulting distribution becomes non-Gaussian due to the relatively slow decline of the wings, even if the original distribution $W(t_N, \phi)$ was Gaussian.

The calculation algorithm is explained in Fig. 5, which shows the original distribution $W(t_N, \phi)$, the new positions of the samples $W(t_N, \phi_k)$ as a result of the phase shift $\Delta\phi_k$ (shown by circles), and the distribution $W(t_0, \phi)$ formed at the end of the time interval τ_{lock}.

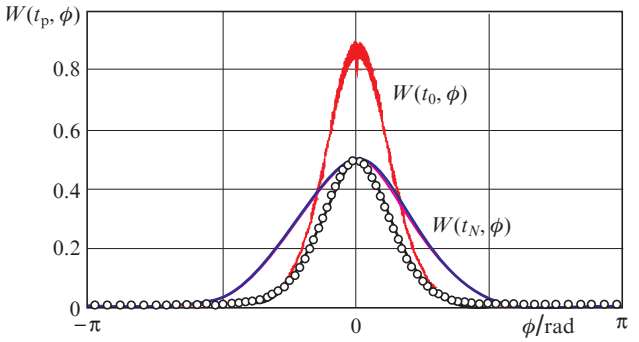

Figure 5. Calculation of the distribution $W(t_0, \phi)$ in the time interval τ_{lock}.

Thus, lock-in plays an important role in preventing the unlimited growth of phase fluctuations and thereby restoring the beat amplitude. Random phases, newly occurring during lock-in, and angular rotation, are not taken into account in the calculation, since the equalisation of random phases generated by lock-in is a faster process than their accumulation caused by spontaneous emission, while the rotation speed, even as significant as 10^5 deg h^{-1}, does not eliminate the effect of equalisation of random phases.

6. Calculation of the integral (total) beat amplitude

The purpose of the calculation and subsequent numerical modelling based on it is to find an explanation for the significant beat amplitude arising from the summation of beats of a large number of PCPWs. In the calculation, we assume that the amplifying medium is a region where, by virtue of a certain mechanism, conditions are created that ensure the synchronicity of the PCPW beats.

We do not consider the mode competition, assuming that it is related to the burnout effect of spatial holes in the SOA. This effect, as we believe, does not occur when using the AFD, since the antinodes and nodes of standing waves are continuously shifted, which leads to the averaging of the carrier distribution in the SOA. We ignore nonlinear processes such as stimulated Brillouin scattering and four-wave mixing, since the number of modes involved in lasing is quite

large, and, therefore the mode intensities are relatively small. We also do not take into acccount the optical losses in the fibre, the semiconductor crystal length due to its smallness, and the total travel length of the output waves from the coupler to the photodetector. As above, we consider the polarisation of all waves to be linear and perform the calculations for discrete time moments t_p, omitting the index p in the formulae below.

Let the exit point of the waves from the RC be located at a distance x (clockwise) and at a distance $L - x$ (counterclockwise) from the SOA centre, taken as the coordinate origin. If we assume that the lock-in zone width in the MSLG does not exceed 1–2 kHz, and the frequency dithering $v_d(t)$ is at least 3 to 5 times higher, then the PCPW beats at the recording point, i.e., in front of the photodetector, can be represented [7] in the form of intensity oscillations with the same frequency equal to the sum of the frequency dithering and the Sagnac signal frequency:

$$I_{ki}(t) = 0.5a_{ki}^2\{1 + \cos\{2\pi[v_S + v_d(t)]t + \Psi_{ki}\}\}, \qquad (13)$$

where a_{ki} is the PCPW amplitude; v_S is the Sagnac frequency; k is the line number in the spectrum; i is the mode number in the line; and Ψ_{ki} is the beat phase, individual for each PCPW.

We represent the beat phases Ψ_{ki} as a sum of two components: the first is determined by different PCPW travel lengths from the antinodes of standing waves, formed by the corresponding PCPW, to the recording point in the SOA, and the second is determined by phase fluctuations. As the antinodes from which the travel lengths of counter-propagating waves are counted, we choose those that are located as close as possible to the coordinate origin.

Thus, the current of the photodetector, at the output of which a radio-frequency filter is located to suppress intermode beats, can be expressed as:

$$i(t) = H\left\{I_0 + \sum_{k,i} a_{ki}^2 \cos\left\{ 2\pi[v_S + v_d(t)]t + \frac{2\pi}{\lambda_{ki}}[nX^+ - nX^- - 2n_s\tilde{h}_{ki}(t)] + \tilde{\xi}(t)\right\}\right\}, \qquad (14)$$

where H is the photodetector sensitivity; $I_0 = 0.5\sum_{k,i} a_{ki}^2$; λ_{ki} are the wavelengths of the modes; $X^+ = x$; $X^- = L - x + 2l_{mir}$; l_{mir} is the length of the coupler port with a mirror at the end face; $\tilde{h}_{ki}(t)$ are the coordinates of antinodes; and $\tilde{\xi}(t)$ is the random phase difference that is statistically the same for all PCPWs.

By performing the trigonometric transformations in (14) and taking into account that the function $W(t_p, \phi)$, even with respect to the phase ϕ, can be considered as a distribution function of the random phase difference $\tilde{\xi}(t)$, and the ratio of the RC optical length and the wavelength for each mode is an integer Q_{ki}, i.e. $nL/\lambda_{ki} = Q_{ki}$, we find the photodetector current averaged over the phase fluctuations:

$$\langle i(t)\rangle = H\left\{I_0 + V_\phi(t)\sum_{k,i} a_{ki}^2 \cos\left\{-2\pi[v_S + v_d(t)] + \frac{2\pi[nX - 2\tilde{h}_{ki}(t)]}{\lambda_{ki}}\right\}\right\}, \qquad (15)$$

where $X = 2(x - l_{mir})$; and

$$V_\phi(t) = \int_{-\pi}^{\pi} \cos\phi\, W(t,\phi)\,d\phi. \qquad (16)$$

Continuing the trigonometric transformations and averaging the coordinates of antinodes, we come to the expression for the photodetector current:

$$\langle i(t)\rangle = HI_0\{1 + V(t,X)\cos\{2\pi[v_S + v_d(t)] + \theta(X)\}\}, \qquad (17)$$

where

$$V(t,X) = V_\lambda(X)\,V_\phi(t); \qquad (18)$$

$$V_\lambda(X) = \left\langle \frac{1}{I_0}\left(\left\{\sum_{k,i} a_{ki}^2 \sin\left\{\frac{2\pi[nX - 2n_s\tilde{h}_{ki}(t)]}{\lambda_{ki}}\right\}\right\}^2 + \left\{\sum_{k,i} a_{ki}^2 \cos\left\{\frac{2\pi[nX - 2n_s\tilde{h}_{ki}(t)]}{\lambda_{ki}}\right\}\right\}^2\right)^{1/2}\right\rangle; \qquad (19)$$

and $\theta(X)$ is the phase equal to the averaged arctangent of the ratio of the two sums in the right-hand side of (19).

Thus, the beat amplitude (18) is determined by the product of the functions $V_\phi(t)$ and $V_\lambda(X)$, the first of which is the average beat amplitude of each individual PCPW, and the second is the result of summing the beats of the PCPW set representing all radiation modes.

7. Results of numerical modelling and their discussion

According to (16), the function $V_\phi(t)$ is determined by the distribution $W(t, \phi)$, which depends on the spectral width of the modes, the backscattering level, and the lock-in duration. Figure 6 shows the functions $V_\phi(t)$ in the time interval τ_{dither} for three values of the mode spectral width $\Delta\nu_{Lm}$, equal to 1, 2, and 4 kHz, all other parameters (L, n, l_s, n_s, γ, v_m, τ_{dither}, and τ_{lock}) retained the values used in previous calculations.

It can be seen that for the mode spectral width equal to 1 and 2 kHz over the entire interval τ_{dither}, the value of func-

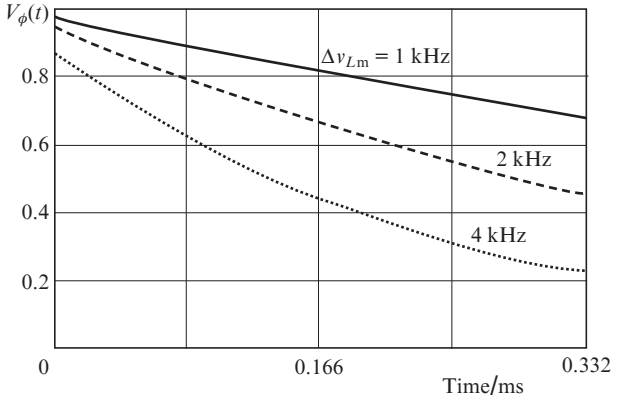

Figure 6. Dynamics of the function $V_\phi(t)$.

tion $V_\phi(t)$, which represents the average beat amplitude of individual PCPWs, is quite large despite its gradual decrease, and the dynamics of this function coincides well with the real dynamics of beats at the MSLG output.

When calculating the function $V_\lambda(X)$, we set and varied the number of lines in the optical spectrum K, their width Λ, the intervals $\Delta\Lambda$ between the lines, the geometric parameter X, the average value $\bar{h}$ of the coordinates of antinodes and their standard deviation σ_h. The last two parameters were used to generate random values of the coordinates of antinodes $\bar{h}_{ki}(t)$, distributed according to the normal law.

We also took into account the instabilities of the optical length nL of the ring cavity and the intervals between the spectrum lines $\Delta\Lambda$, caused by temperature fluctuations and other factors. To this end, for given standard deviations σ_{nL} and $\sigma_{\Delta\Lambda}$, random values $\delta(nL)$ and $\delta\Delta\Lambda$ were generated, which were used to calculate a set of wavelengths λ_{ki} satisfying the relation $nL/\lambda_{ki} = Q_{ki}$.

From the calculation results, it follows that the function $V_\lambda(X)$ is even, has a maximum value at $X = 0$, and decreases sharply with increasing linewidth Λ and standard deviation σ_h. Figure 7 shows the results of calculating the function $V_\lambda(X)$ for several variants of the values Λ and σ_h for $K = 4$, $\sigma_{nL} = 10^{-3}nL$, and $\sigma_{\Delta\Lambda} = 10^{-3}\Delta\Lambda$.

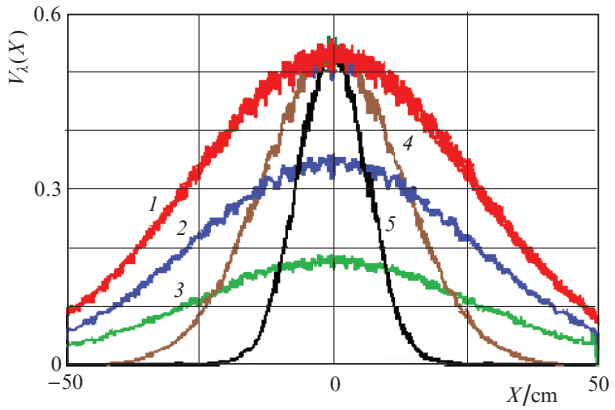

Figure 7. Function $V_\lambda(X)$ at (*1*) $\Lambda = 0.001$ nm, $\sigma_h = 0.01\lambda_0$; (*2*) $\Lambda = 0.001$ nm, $\sigma_h = 0.05\lambda_0$; (*3*) $\Lambda = 0.001$ nm, $\sigma_h = 0.08\lambda_0$; (*4*) $\Lambda = 0.002$ nm, $\sigma_h = 0.01\lambda_0$; and (*5*) $\Lambda = 0.004$ nm, $\sigma_h = 0.01\lambda_0$; $\lambda_0 = 1.55$ μm.

Note also that the function $V_\lambda(X)$ does not depend on the average value $\bar{h}$ of the coordinates of antinodes and the intervals $\Delta\Lambda$ between the lines, but depends on the number K of lines: it is quite large for a small number of lines and decreases significantly when the number of lines exceeds 10. The instabilities of the optical length $\delta(nL)$ and the intervals between the lines $\delta\Delta\Lambda$ smooth out the oscillations of the function $V_\lambda(X)$, which would be quite considerable in their absence.

Thus, from the presented results it follows that sufficiently large values of the function $V_\lambda(X)$ are observed if four parameters (number of lines M in the optical spectrum, geometric parameter X, spectral linewidth $\Delta\Lambda_k$, and the standard deviation σ_h of the coordinates of antinodes) simultaneously have small values, with, the latter parameter being small at any time moment.

Small values of the parameters M and X are easily achieved by limiting the SOA pump current and selecting the appropriate value of l_{mir}, while small values of the standard deviation σ_h and linewidth $\Delta\Lambda_k$ are set by themselves.

The smallness of σ_h means that the positions of antinodes and nodes of standing waves in the SOA, formed by the modes of each line of the spectrum, coincide exactly or with small deviations. Hence, in turn, it follows that the RC modes belonging to the same line of the optical spectrum are synchronised. Since the fibre dispersion at a moderate RC length, which we used, virtually does not affect the phase velocity of the mode propagation, mode locking is observed not only in the SOA, but also at each RC point, and constantly.

The mode locking in the MSLG is not identical to the phenomenon of the same name used in the technique of ultrashort radiation pulses, but represents a hitherto unknown lasing mode. We believe that, in this case, there is not a simple equality of phases, but a certain relationship between the phases of waves propagating in one direction, in which the phase difference for all pairs of waves at any time moment remains an integral multiple of the value 2π, while the phases of the waves periodically jump or rapidly increase or decrease by 2π.

The nature of mode locking is illustrated in Fig. 8, which shows the phase dynamics of five waves propagating in the same direction. The phase dynamics of the wave that is part of the central mode of the kth line is represented by the straight line $\Phi_{k0}(t) = \omega_{k0}t$, where ω_{k0} is the average spectral line frequency. The phase dynamics of the other four waves representing adjacent modes is described by piecewise linear functions with linear sections parallel to the given straight line and fast transitions (jumps) from one linear section to another; the time intervals corresponding to the linear sections are the smaller, the more the mode frequency differs from the frequency ω_{k0}.

The dynamics under consideration refers to the steady-state operation regime, since it is obvious that at the initial stage, the positions of the antinodes of standing waves are

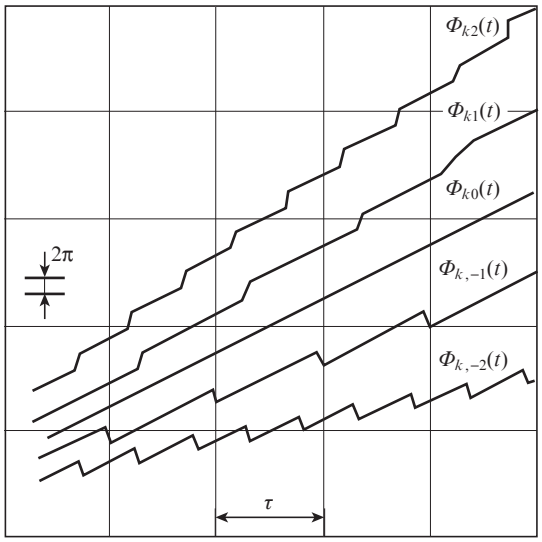

Figure 8. Five-wave phase dynamics explaining the mode locking in the MSLG.

random, and the optical spectrum is unlikely to consist of narrow lines. The mechanism of the steady-state regime formation is unclear: we believe that it is due to the uniform broadening of spectral lines, the interaction of modes in the amplifying medium, the small spectral width of the modes, and the small intermode spacing.

8. Conclusions

We have described the design and research results of an MSLG with an optical fibre as a RC and frequency dithering formed using a lithium niobate phase modulator, and also considered the factors that determine the operability of this device.

The fundamental limitations in the MSLG operation are phase fluctuations caused by spontaneous emission of photons and the multimode nature of the generated radiation. Factors that reduce the rigidity of both constraints include the large ring cavity length, the alternating frequency dithering, the small spectral mode width, and, as a consequence, the low level of phase fluctuations. The latter, however, gradually accumulate, causing a slow drop in the beat amplitude. However, its complete decay does not occur due to periodic and short-term lock-in, which leads to equalisation, to one degree or another, of the difference in phase fluctuations of the counterpropagating waves that form the cavity modes, and thereby restores the beat amplitude.

The main factors that make it possible to overcome the limitations associated with the multimode lasing regime are small number of narrow lines in the emission spectrum and mode locking in the optical spectrum lines. The mode locking in the MSLG is not identical to the well-known phenomenon of the same name; the mechanism of its occurrence and the mechanism of formation of narrow lines have not yet been established and require further research.

Acknowledgements. The author is grateful to L.P. Prokofyeva and V. V. Shcherbakov for their attention to this work.

References

1. Taguchi K., Fukushima K., Ishitani A., Ikeda M. *Electron. Lett*., **34**, 1775 (1998).
2. Inagaki K.,Tamura S., Noto H., Harayama T. *Phys. Rev. A*, **78**, 53822 (2008).
3. Mignot A., Feugnet G., Schwartz S., et al. *Opt. Lett.*, **9**, 34 (2009).
4. Akparov V.V., Dmitriev V.G., Duraev V.P., Kazakov A.A. *Quantum Electron*., **40**, 851 (2010) [*Kvantovaya Elektron*., **40**, 851 (2010)].
5. Sakharov V.K. *Zh. Tekh. Fiz*., **81** (8), 76 (2011).
6. Prokofyeva L.P., Sakharov V.K., Shcherbakov V.V. *Quantum Electron*., **44**, 362 (2014) [*Kvantovaya Elektron*., **44**, 362 (2014)].
7. Sakharov V.K. *Quantum Electron*., **46**, 567 (2016) [*Kvantovaya Elektron*., **46**, 567 (2016)].
8. Sakharov V.K., Mashinskiy S.S. *Proc. Conf. VKVO-19* (Perm, 2019) p. 34.
9. Henry C. *IEEE J. Quantum Electron.*, **18**, 259 (1982).
10. Sakharov V.K.,Vasilyev M.G. *Laser Phys*., **10**, 857 (2000).